ELSEVIER

Nuclear Physics B (Proc. Suppl.) 94 (2001) 461–468

NUCLEAR PHYSICS B
PROCEEDINGS
SUPPLEMENTS
www.elsevier.nl/locate/npe

Numerical study of dense adjoint 2-color matter*

Simon Hands[a], István Montvay[b], Manfred Oevers[c †], Luigi Scorzato[a] and Jonivar Skullerud[b]

[a]Department of Physics, University of Wales Swansea, Singleton Park, Swansea SA2 8PP, Wales

[b]Theory Division, DESY, Notkestraße 85, D-22603 Hamburg, Germany

[c]Department of Physics and Astronomy, University of Glasgow, Glasgow G12 8QQ, Scotland

We study the global symmetries of SU(2) gauge theory with N flavors of staggered fermions in the presence of a chemical potential. We motivate the special interest of the case $N = 1$ (staggered) with fermions in the adjoint representation of the gauge group. We present results from numerical simulations with both hybrid Monte Carlo and the Two-Step Multi-Bosonic algorithm.

1. INTRODUCTION

QCD at finite baryonic density is expected to display a rich phase diagram [1]. Unfortunately numerical simulations at non zero density are still prohibitive because of the sign problem (for a review of the recent progress on that matter see [2]). The finite density sector can be studied numerically in a class of theories which includes any SU(2) gauge theory. In such cases, in fact, the fermionic determinant is real (and positive for an even number of flavors). All these theories can also be studied by means of Chiral Perturbation Theory (χPT) even in the finite density region [3]. Here χPT predicts the presence of some Goldstone modes associated with spontaneous chiral symmetry breaking which are sensitive to the chemical potential, and can therefore be called *diquark* or *baryonic* Goldstone modes. These modes drive the onset transition between the low and the high density regime which appears when μ is of the order of the pion mass $m_\pi \sim \sqrt{m}$. The same features that ensure that the fermionic determinant is real are also related to the prediction of an early onset transition. It is therefore interesting to note that there is a special case: the SU(2) gauge theory with one flavor of staggered fermions in the adjoint representation of the gauge group ($\mathrm{SU}(2)_{\mathrm{Adj}}^{N=1\,\mathrm{stagg}}$ [4]) which has a real fermionic determinant, but where no baryonic Goldstone modes are expected. It is therefore an ideal model to explore the influence of the sign on the observables and on the pattern of symmetry breaking. We will give numerical evidence that this model, if constrained to the sector with positive determinant, still belongs to the class of theories with baryonic Goldstone modes. Then we show how the inclusion of the sign changes this picture, suggesting a delayed onset transition.

As a by-product we gain important experience with two numerical algorithms when $\mu \neq 0$: the hybrid Monte Carlo (HMC) and Two-Step Multi-Bosonic algorithms.

2. SYMMETRIES

We first present the continuum and lattice formulation of Two Color QCD. The fermionic part of the action for N_f flavors f in the continuum is:

$$S_F = \int d^4x\, \bar{\psi}^f(x)(\partial_\nu + igA_\nu + \mu\delta_{\nu 0})\gamma_\nu \psi^f(x) \quad (1)$$

The lattice action for staggered fermions is

$$\begin{aligned} S_F &= \sum_{x,y} \bar{\chi}^p(x)\big(D_{xy}[U,\mu] + m\delta_{xy}\big)\chi^p(y) \\ &\equiv \sum_{x,y} \bar{\chi}^p(x) M_{xy}[U,\mu]\chi^p(y)\,, \end{aligned} \quad (2)$$

*Material based on talks by L. Scorzato and J. Skullerud.
†Current address: IBM UK, 1 New Square, Bedfont Lakes, Feltham, Middx, TW14 8HB, UK

PII S0920-5632(01)01007-6

where the index p runs over N flavors of staggered quark, and D is given by

$$D_{xy} = \sum_{\nu\neq 0} \frac{\eta_\nu(x)}{2}\left(U_\nu(x)\delta_{x,y-\hat{\nu}} - U_\nu^\dagger(y)\delta_{x,y+\hat{\nu}}\right) + \frac{\eta_0(x)}{2}\left(e^{\mu}U_0(x)\delta_{x,y-\hat{0}} - e^{-\mu}U_0^\dagger(y)\delta_{x,y+\hat{0}}\right) \quad (3)$$

$\chi, \bar{\chi}$ are single spin component Grassmann objects, and the phases $\eta_\mu(x)$ are defined to be $(-1)^{x_0+\cdots+x_{\mu-1}}$. For brevity, we have here used U to denote both the fundamental (2×2 complex unitary) and adjoint (3×3 real orthogonal) link fields.

2.1. Sign of the determinant

As is well known, Two Color QCD has a real fermionic determinant also at non zero density. In fact the SU(2) group only has real or pseudoreal representations. For all such representations it is always possible to find a unitary operator T such that KT commutes with the fermionic matrix M, where K is the complex conjugate operator. If such an operator exists one can show [3,5] that all the eigenvalues of M appear in complex conjugate pairs and thus the determinant of M must be real. Although for the theories we are considering here $\det M$ is real, it need not be positive definite. Indeed, it turns out that some of these theories have a sign problem. It can be shown [3,5] that a sufficient condition for a positive definite action is that there is one choice of T such that $(KT)^2 = -1$.

For the continuum action, given by (1), one finds

$$\begin{aligned} &\text{fundamental:} \quad T = C\gamma_5 \otimes \tau_2, \ \ (KT)^2 = 1\,; \\ &\text{adjoint:} \quad T = C\gamma_5 \otimes \mathbb{I}, \ \ (KT)^2 = -1\,. \end{aligned} \quad (4)$$

Here, C is the charge conjugation matrix. For staggered lattice fermions M is given by (2,3), and

$$\begin{aligned} &\text{fundamental:} \quad T = \tau_2, \ \ (KT)^2 = -1\,; \\ &\text{adjoint:} \quad T = \mathbb{I}, \ \ (KT)^2 = 1\,. \end{aligned} \quad (5)$$

We thus have a proof that the functional integral measure is positive definite for continuum adjoint quarks and fundamental staggered quarks. There is no such proof for continuum fundamental quarks and staggered adjoint quarks, and as we shall demonstrate in section 4.4, there are indeed isolated real eigenvalues and hence a sign problem for the adjoint staggered model at large chemical potential μ.

2.2. Symmetry breaking pattern

In the chiral limit, the action has a $\mathrm{U}(N)_L \otimes \mathrm{U}(N)_R$ symmetry, which for staggered fermions is manifest as independent $\mathrm{U}(N)$ symmetries for the even and odd sites. At $\mu = 0$ this enlarges to a $\mathrm{U}(2N)$ symmetry. This can be seen most easily by introducing new fields,

$$\bar{X}_e = (\bar{\chi}_e, -\chi_e^{\mathrm{tr}}\tau_2) \qquad X_o = \begin{pmatrix} \chi_o \\ -\tau_2\bar{\chi}_o^{\mathrm{tr}} \end{pmatrix} \quad (6)$$

for fundamental quarks, and

$$\bar{X}_e = (\bar{\chi}_e, \chi_e^{\mathrm{tr}}) \qquad X_o = \begin{pmatrix} \chi_o \\ \bar{\chi}_o^{\mathrm{tr}} \end{pmatrix} \quad (7)$$

for adjoint quarks. The action can then be written as

$$S = \frac{1}{2}\sum_{x\,\mathrm{even},\nu} \eta_\nu(x)\left(L_+(x) - L_-(x)\right) \quad (8)$$

where

$$L_+ = \bar{X}_e(x)\begin{pmatrix} e^{\mu\delta_{\nu,0}} & \\ & e^{-\mu\delta_{\nu,0}} \end{pmatrix} U_\nu(x)X_o(x+\hat{\nu}) \quad (9)$$

$$L_- = \bar{X}_e(x)\begin{pmatrix} e^{-\mu\delta_{\nu,0}} & \\ & e^{\mu\delta_{\nu,0}} \end{pmatrix} U_\nu^\dagger(x-\hat{\nu})X_o(x-\hat{\nu}) \quad (10)$$

In the continuum, the equivalent fields are

$$\text{fundamental:} \qquad \Psi = \begin{pmatrix} \psi_L \\ \sigma_2\tau_2\psi_R^* \end{pmatrix} \quad (11)$$

$$\text{adjoint:} \qquad \Psi = \begin{pmatrix} \psi_L \\ \sigma_2\psi_R^* \end{pmatrix} \quad (12)$$

which gives the lagrangian

$$\mathcal{L} = i\Psi^\dagger\sigma_\nu(D_\nu - \mu B_\nu)\Psi \quad (13)$$

where

$$B_\nu = B\delta_{\nu 0}\,; \qquad B = \begin{pmatrix} 1 & 0 \\ 0 & -1 \end{pmatrix} \quad (14)$$

The chiral condensate can be written in terms of the new fields,

$$\bar{\chi}\chi = \bar{X}_e \begin{pmatrix} \mathbb{I} & \\ & \pm\mathbb{I} \end{pmatrix} \frac{T}{2} \bar{X}_e^{tr} + X_o^{tr} \begin{pmatrix} \mathbb{I} & \\ & \pm\mathbb{I} \end{pmatrix} \frac{T}{2} X_o \quad (15)$$

where the + sign is for fundamental fermions and the − sign for adjoint, while T is the unitary operator defined in section 2.1. A nonzero chiral condensate thereby breaks down the U($2N$) symmetry to O($2N$) for fundamental fermions and Sp($2N$) for adjoint fermions, giving rise to $N(2N+1)$ and $N(2N-1)$ Goldstone modes respectively. Of these, there will be N^2 mesonic states, while the remaining $N(N \pm 1)$ will be diquarks. From this we see that in the case of $N = 1$ adjoint fermions, and only in this case, are there no diquark Goldstone modes.

For $m \neq 0$, all states remain degenerate, gaining masses $m_\pi \propto \sqrt{m}$ in accordance with standard PCAC arguments. As the chemical potential μ increases from zero, a ground state containing baryonic matter is promoted, signalled by a non-zero value for the baryon number density

$$n = \frac{1}{2}\langle \bar{\chi}(x)\eta_0(x)[e^{\mu}U_0(x)\chi(x+\hat{0}) + e^{-\mu}U_0^{\dagger}(x-\hat{0})\chi(x-\hat{0})]\rangle. \quad (16)$$

At zero temperature n thus serves as an order parameter for an *onset* phase transition occuring at some μ_o separating the vacuum from a state containing matter. A naive energetic argument would suggest that the onset transition should occur for a value of μ_o equal to the mass per baryon charge of the lightest particle carrying non-zero baryon number. For the models discussed in the previous paragraph in which some of the Goldstone modes are diquark states, those states will be the lightest baryons in the spectrum. This means that for most variants of Two Color QCD we expect $\mu_o \simeq m_\pi/2$, in contrast to the much larger value $m_N/3$ expected in physical QCD. The exception is $\mathrm{SU}(2)^{N=1\mathrm{stagg}}_{\mathrm{Adj}}$.

3. ALGORITHMS

We have studied Two Color lattice QCD with $N = 1$ adjoint flavors of staggered fermions, using two different simulation algorithms: the hybrid Monte Carlo (HMC) algorithm [6], and a Two-Step Multi-Bosonic (TSMB) algorithm [7]. In [5] we described in detail how both algorithms are defined for the model above. Here we only remind that, in order to optimise the performances, in both cases we need to tune the simulation parameters. In HMC we tuned the mean trajectory length and the size of the discretised time step. In TSMB we have a larger set of parameters: the interval $[\epsilon, \lambda]$ over which the polynomial approximation is performed, the degrees of the four polynomials (n_i, $i = 1, \ldots, 4$), and the number of Metropolis, heatbath and overrelaxation iterations for the gauge and the boson fields respectively.

The first observation is that as the ratio $\mu/\sqrt{m}$ increases some eigenvalues of the fermionic matrix approch zero and any simulation becomes hard in that region. By increasing $\mu/\sqrt{m}$ further, some eigenvalues get a negative real part. It turns out that the model allows configurations with a negative determinant (when an odd number of real negative eigenvalues appear). At this point TSMB and HMC display different behaviours. TSMB simulations can easily sample configurations with both signs of $\det M$, for any combination of the simulation parameters that we used. HMC simulations (at least for the combinations of trajectory lengths and time steps that we used, which are dictated by efficiency considerations) were never able to change the sign of $\det M$.

The reason for this difference must reside in the updating of the gauge fields, since $\det M$ is only defined in term of these. In the case of HMC the accept/reject step is performed only after updating the whole configuration and the exact action is used. In the case of TSMB the gauge field updating is performed by a Metropolis algorithm and the action is given by a polynomial approximation realised by means of auxiliary boson fields. These conditions apparently allow TSMB to change the sign of $\det M$ more easily than HMC. The exactness of the TSMB algorithm is guaranteed by a final reweighting step, which is necessary since no polynomial approximation is sufficient when dealing with arbitrarily small eigenvalues.

Table 1
Integrated autocorrelation of the plaquette τ_{int}^{plaq} for TSMB and HMC at $\beta = 2.0$, $m = 0.1$, $\mu = 0.0$ on a $4^3 \times 8$ lattice. For TSMB we use polynomial orders: n_1, $n_2 = 90$, $n_3 = 120$; interval of approximation: $[\epsilon = 0.005, \lambda = 10.0]$. For both algorithms R_{acc} is the acceptance rate of the correction step, and N_{sweep} is the length of runs in sweeps or trajectories. N_{mult} is the number of matrix multiplications per sweep. N_{int}^{plaq} is the autocorrelation in number of matrix multiplications.

Alg.	n_1	R_{acc}	N_{sweep}	τ_{int}^{plaq}	N_{mult}	N_{int}^{plaq}	$\langle\Box\rangle$
TSMB	24	0.68	283000	420(20)	1500	$6.30 \cdot 10^5$	0.5676(8)
TSMB	24	0.68	110000	430(35)	500	$2.15 \cdot 10^5$	0.5687(10)
TSMB	16	0.32	195000	360(30)	460	$1.66 \cdot 10^5$	0.5684(7)
HMC	-	0.83	35000	10	19500	$1.9 \cdot 10^5$	0.5682(4)

4. RESULTS

4.1. Autocorrelation studies

In order to establish the errors of our numerical studies we analysed the autocorrelation times of both algorithms and expressed them in the common unit of measure of *matrix multiplications* (appropriately corrected with a factor that takes into account that TSMB spends more time in other kinds of operation). The number of matrix multiplications per sweep is a function of the parameters of the simulation [5]. It turns out, in general, that the gluonic observables have a much longer autocorrelation time than the fermionic ones, sometimes by even two orders of magnitude. In the following we will consider only the former, in order to be conservative. At zero density we could determine the autocorrelation time with sufficient precision for both algorithms. The results are shown in table 1. The runs in the table are sufficiently long for the measurement of the integrated autocorrelations. The run in the first line has relatively more gauge update sweeps compared to the boson field updates: it has $N_M = 12$ Metropolis gauge sweeps per $N_H = 2$ heatbath and $N_O = 1$ overrelaxation bosonic sweeps. This is obviously not advantageous for the autocorrelation. In the other two runs $N_M = 4$ which is substantially better. The difference between the second and third lines is in the number of auxiliary boson fields (equal to the rank of the first polynomial). The table shows that a low acceptance about 30% is somewhat better than the higher one near 70%. Further optimisation of the choice of TSMB parameters in this point is still possible but N_{int}^{plaq} is already smaller than the corresponding number in HMC.

Our longest TSMB run at $\mu = 0.4$ is not long enough for an accurate determination of the integrated plaquette autocorrelation. After 80000 sweeps (on a $4^3 \times 8$ lattice) the obtained autocorrelation estimate is $\tau_{int}^{plaq} \simeq 2400$ ($N_{int}^{plaq} \simeq 6 \cdot 10^6$). The obtained result is good enough for an order of magnitude estimate of τ_{int}^{plaq} but the real value may be somewhat larger. Also in the case of HMC, the longest run of 18000 trajectories was not sufficient to determine the autocorrelation.

Since the point at $\mu = 0.4$ appears so difficult, we started an analysis of autocorrelation at point $\mu = 0.36$. Our longest run (40000 sweeps) is still too short to provide an accurate determination. However we can at least estimate the order of magnitude of $\tau_{int}^{plaq} \simeq 500$ ($N_{int}^{plaq} \simeq 8 \cdot 10^5$).

4.2. Reweighting

The final precision in the TSMB algorithm is achieved by reweighting the gauge configurations at the evaluation of expectation values. In a model with $\det M$ possibly negative, as considered here, the sign of the determinant is also taken into account in the reweighting. The choice of the order of the second polynomial n_2 has an important effect on the reweighting. For sufficiently large n_2 the two-step approximation can be so good that the effect of reweighting is negligible compared to the statistical errors. In fact, this

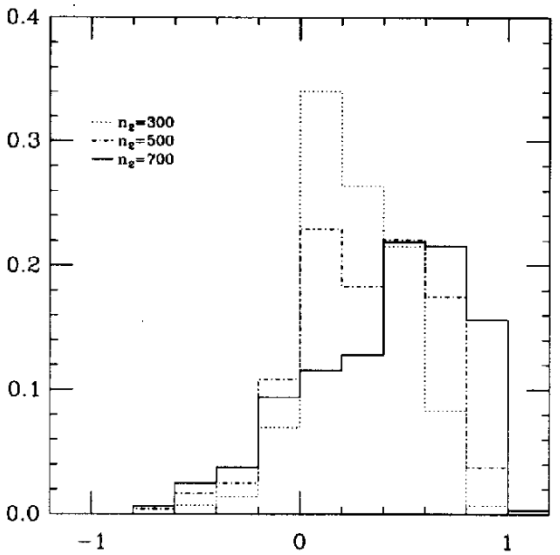

Figure 1. Examples of reweighting factors for different choices of the second polynomial, at $\beta = 2.0, m = 0.1, \mu = 0.36$ with $n_1 = 64$.

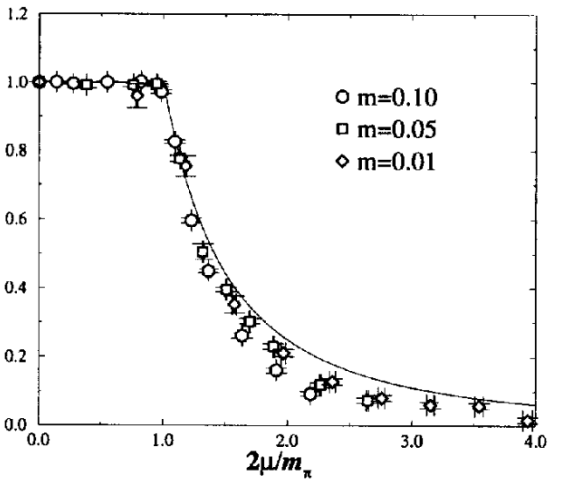

Figure 2. Chiral condensate vs. chemical potential using the rescaled variables of eq. (17).

ideal situation can be achieved in the low density phase of our model where negative determinants practically never occur. In the high density phase, however, negative determinants play an important rôle and it is more advantageous to have a non-negligible reweighting. (This is also required by the very small eigenvalues which can be treated exactly in the reweighting step.) Of course, a very low value of n_2 is not optimal either because then the typical reweighting factors become too small and the effective statistics is substantially reduced. The effect of choosing the order of the second polynomial on the distribution of reweighting factors is shown by fig. 1.

4.3. Physics results from HMC

We used three distinct quark masses on the $4^3 \times 8$ lattice at $\beta = 2.0$, and explored values of μ up to and including 0.8 for $m = 0.1$, $\mu = 0.7$ for $m = 0.05$, and $\mu = 0.5$ for $m = 0.01$.

Here we measured the chiral condensate $\langle\bar{\chi}\chi\rangle$ the baryon number density n (16), the plaquette and the pion mass m_π. If we define the rescaled variables $x = 2\mu/m_{\pi 0}$, $y = \langle\bar{\chi}\chi\rangle/\langle\bar{\chi}\chi\rangle_0$, and $\tilde{n} = m_{\pi 0} n / 8m\langle\bar{\chi}\chi\rangle_0$ (where the 0 subscript denotes values at zero chemical potential), then χPT predicts (in the limit of small m and μ) that all data should fall on the lines [3]

$$y = \begin{cases} 1 & x<1 \\ \frac{1}{x^2} & x>1 \end{cases} \qquad \tilde{n} = \begin{cases} 0 & x<1 \\ \frac{x}{4}\left(1-\frac{1}{x^4}\right) & x>1 \end{cases} \tag{17}$$

In Figs 2 and 3 we show the rescaled variables y and $\tilde{n}$ respectively as functions of x. The data collapse very nicely onto a universal curve, corresponding quite closely to the prediction (17). The systematic departures from the theoretical curves for $x < 2$, downwards for the condensate data and upwards for the baryon density, may well be explicable by higher order corrections in χPT. Our more recent results from the regime $x > 2$, however, suggest a dispersion in the data from different m, and hence a possible breakdown of χPT at higher densities. This may be due to new thresholds as particles other than Goldstones are induced into the ground state, or even a further phase transition [5].

Whilst the approximate quantitative agreement between our results and the theoretical predictions of [3] is gratifying, it also contradicts the symmetry-based arguments of section 2 that there are no baryonic Goldstones for $N = 1$ staggered flavor, and no gauge-invariant local diquark

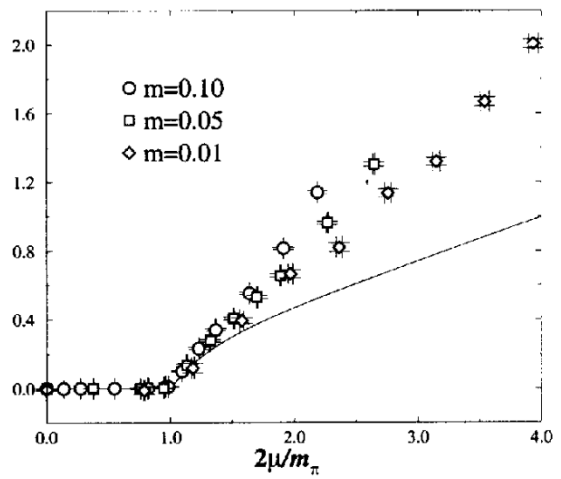

Figure 3. Baryon density vs. chemical potential using the rescaled variables of eq. (17).

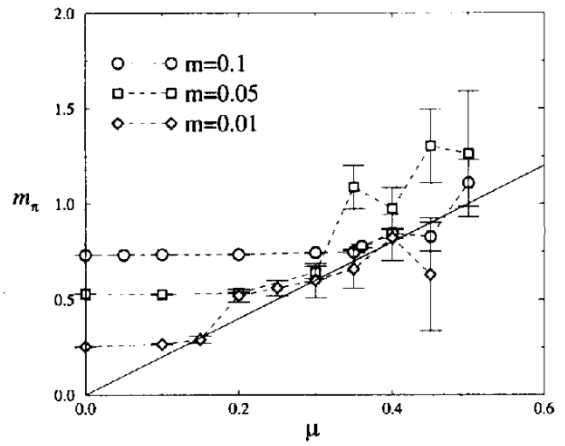

Figure 4. m_π vs. μ, for the three different quark masses. Also shown is the line $m_\pi = 2\mu$.

condensate. We believe that this is because the HMC simulations fail to take account of the determinant sign (or indeed even to change it) ie. that simulations with functional weight $|\det M|$ yield broadly similar results to those with weight $\det^2 M$. The premature onset at $\mu_o = m_\pi/2$ is therefore a direct manifestation of the sign and/or ergodicity problems.

In Fig. 4 we show results for m_π, obtained using a standard cosh fit to the meson correlator over all 8 timeslices. The fits are quite stable in the low density phase, but the correlators become very noisy once $n > 0$, resulting in a much reduced precision. It is significant, however, that our results in the dense phase are at least consistent with the χPT prediction $m_\pi = 2\mu$ [3].

Finally we turn to the effect of the chemical potential on the gauge fields. Since this can only be communicated via fermion loops, any effect we see can be ascribed with certainty to dynamical fermions. Gluonic observables, however, are also much more prone to auto-correlations as described in section 4.1, particularly as the quark mass is reduced. Systematic changes with μ are therefore quite difficult to observe. In this initial HMC study we have only measured the average plaquette; the results are shown in Fig. 5. The data for $m = 0.1$ show the plaquette remaining roughly constant for $\mu < \mu_o$, before beginning to decrease. The points for $m = 0.05, 0.01$ have been omitted for clarity, but reveal a similar picture. We interpret it as follows: for temperature $T = 0$, all values of $\mu < \mu_o$ are physically equivalent corresponding to the same physical state, namely the vacuum. We only expect an effect on gluonic observables in the presence of matter, ie. for $\mu > \mu_o$. To the extent that the results are constant for $\mu < \mu_o$ we can be confident that our simulation has an effective $T \simeq 0$. The decrease in the plaquette for $\mu > \mu_o$ may be due to the decrease in the number of virtual quark–anti-quark pairs which may form due to the Exclusion Principle — an effect known as *Pauli blocking*. This results in a decrease of screening via vacuum polarisation, and hence an effective renormalisation of the gauge coupling β and consequent decrease of the plaquette. In the large-μ limit the lattice should become saturated with one quark of each color per site, and the plaquette assume its quenched value [4].

4.4. Physics results from TSMB

Each TSMB simulation is characterised by a vector n_i specifying the polynomial orders at each stage, as described in [7]. For each configuration generated, a reweighting factor r and the sign

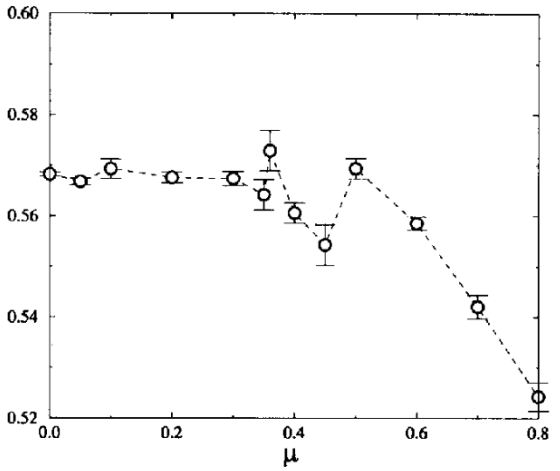

Figure 5. Average plaquette vs. μ for $m = 0.1$.

Table 2
Parameters for the TSMB simulations. $N_{\rm cfg}$ is an estimate of the number of independent configurations, using the estimates of the autocorrelation time from section 4.1.

μ	(n_1, n_2)	$N_{\rm cfg}$	$\langle r \times sign \rangle$
0.0	(16,100)	90	
0.36	(64,500)	120	0.313(20)
	(64,700)	160	0.417(21)
0.4	(100,1000)	128	0.030(59)

of $\det M$ must be determined. On the relatively small lattices considered here, we have been able to compute $\det M$ directly using standard numerical methods. The expectation value of an observable O is then determined by the ratio

$$\langle O \rangle = \frac{\langle O \times r \times sign \rangle}{\langle r \times sign \rangle}. \qquad (18)$$

Here we present results from runs performed on a $4^3 \times 8$ lattice with $\beta = 2.0$, $m = 0.1$ and three values of μ. The parameters are given in table 2. Note that the polynomial orders required increase with μ. The point at $\mu = 0$ was chosen to enable the TSMB algorithm to be tested against HMC, since both should yield identical results. The $\mu \neq 0$ points were chosen so as to have one value just past the HMC onset transition, where the edge of the eigenvalue distribution just overlaps the line $\mathrm{Re}\lambda = 0$ and a small percentage of negative determinant configurations are expected, so that hopefully the sign problem is not too severe, and one value fairly deep in the high density phase.

Our results for the standard observables, together with the corresponding HMC results, are summarised in Table 3. For TSMB at $\mu \neq 0$ we also include observables determined separately in each sign sector, defined by $\langle O \rangle_\pm = \langle O \times r \rangle_\pm / \langle r \rangle_\pm$. We note that the agreement between HMC and TSMB at $\mu = 0.0$ is good, as it should be. The results at $\mu = 0.4$ have too large errors and we cannot derive any conclusion. The results at $\mu = 0.36$ show an acceptable agreement between HMC and the positive sector of TSMB. However, the results for the negative determinant sector are significantly different. (A similar trend may be seen at $\mu = 0.4$, but here the difference is still within 2σ, and thus not statistically significant.) The effect of the sign on the total average — especially for the baryon density — is quite interesting. Even if the errors are still large, we can see that n is already definitely non zero in the positive sector. The inclusion of the negative sector has the effect of bringing back the average n to zero — although it should be pointed out that the TSMB average is also still only about 2σ away from the HMC result. This mechanism is nontrivial since at that point there are very few configurations with negative determinant. For the chiral condensate, the effect of the sign is qualitatively similar in that the inclusion of the sign counteracts the suppression observed in HMC — but we are unable at this stage to draw any quantitative conclusions.

These observations suggest that at this value of μ the system is still in the low density phase, and hence $\mu_{\rm o\ TRUE} > \mu_{\rm o\ HMC}$. This is in accord with our symmetry-based arguments that for $N = 1$ flavors of adjoint staggered fermion there are no baryonic Goldstones and hence no early onset.

5. CONCLUSIONS

We presented our progress in the numerical study of $\mathrm{SU}(2)_{\rm Adj}^{N=1\ \rm stagg}$. We have seen that when

Table 3
A comparison of results between TSMB and HMC. At $\mu = 0.0$ reweighting was not necessary. Due to the long autocorrelation times, the errors in the HMC results, especially for the plaquette, are probably underestimated.

	μ	TSMB			HMC
		$\langle O \rangle$	$\langle O \rangle_+$	$\langle O \rangle_-$	
$\langle \bar{\chi}\chi \rangle$	0.0	1.525(3)			1.526(1)
	0.36	1.551(10)	1.521(8)	1.176(37)	1.485(9)
	0.4	2.49(261)	1.31(4)	1.19(4)	1.253(10)
n	0.0	0.0000(13)			−0.0002(3)
	0.36	−0.0003(80)	0.0199(64)	0.252(32)	0.0172(28)
	0.4	−0.65(179)	0.14(3)	0.23(3)	0.1667(90)
$\Box$	0.0	0.5681(8)			0.5682(4)
	0.36	0.5607(9)	0.5605(8)	0.5580(16)	0.5729(40)
	0.4	0.635(149)	0.5656(16)	0.5584(17)	0.5612(30)
m_π	0.0	0.7321(10)			0.7327(4)
	0.36	0.768(35)	0.798(23)	1.40(71)	0.7778(88)
	0.4	2.14(374)	1.30(40)	0.95(19)	0.8712(34)

the model is constrained to the sector with positive determinant it displays a good agreement with the expectations of χPT. The departure from χPT at large density is now more clear and deserves further investigation. We also confirmed, with narrower errorbars, the presence of a delayed onset when the full model is taken into account. We learnt how to perform a numerical analysis of this difficult model through the use of a TSMB algorithm which is well suited to sample correctly the sign. In future we shall also study the diquark condensates suggested in [5] in order to understand fully the effect of the sign in the region of the parameters where this is possible.

ACKNOWLEDGEMENTS

This work is supported by the TMR-network "Finite temperature phase transitions in particle physics" EU-contract ERBFMRX-CT97-0122. LS thanks the Royal Society for the benefit of a conference grant. Numerical work was performed using a Cray T3-E at NIC, Jülich and an SGI Origin2000 in Swansea.

REFERENCES

1. M. Alford, K. Rajagopal and F. Wilczek, Phys. Lett. B422 (1998) 247, Nucl. Phys. B537 (1999) 443;
R. Rapp, T. Schäfer, E.V. Shuryak and M. Velkovsky, Phys. Rev. Lett. 81 (1998) 53.
2. S. Chandrasekharan, these proceedings.
3. J. Kogut, M.A. Stephanov, D. Toublan, J.J.M. Verbaarschot and A. Zhitnitsky, Nucl. Phys. B582 (2000) 477.
4. S.J. Hands and S.E. Morrison, proceedings of "Understanding Deconfinement in QCD", D. Blaschke *et al.* (eds.), p.31 [hep-lat/9905021].
5. S. Hands *et al.*, Eur. Phys. J. C, DOI 10.1007/s100520000477; hep-lat/0006018.
6. S. Duane *et al.*, Phys. Lett. B195 (1987) 216.
7. I. Montvay, Nucl. Phys. B466 (1996) 259.